COMMUNICATIONS IN NUMERICAL METHODS IN ENGINEERING
Commun. Numer. Meth. Engng (2009)
Published online in Wiley InterScience (www.interscience.wiley.com). DOI: 10.1002/cnm.1250

Detecting corpus callosum abnormalities in autism subtype using planar conformal mapping

Ye Duan[1], Qing He[1,*,†], Xiaotian Yin[2], Xianfeng Gu[2], Kevin Karsch[1] and Judith Miles[3]

[1]*Department of Computer Science, University of Missouri-Columbia, Columbia, MO 65211, U.S.A.*
[2]*State University of New York at Stony Brook, Stony Brook, NY 11794, U.S.A.*
[3]*Thompson Center for Autism, University of Missouri-Columbia, Columbia, MO 65211, U.S.A.*

SUMMARY

A number of studies have documented that autism has a neurobiological basis, but the anatomical extent of these neurobiological abnormalities is largely unknown. In this paper, we apply advanced computational techniques to extract 3D models of the corpus callosum (CC) and subsequently analyze local shape variations in a homogeneous group of autistic children. Besides the traditional volumetric analysis, we explore additional phenotypic traits based on the oriented bounding rectangle of the CC. In shape analysis, a new conformal parameterization is applied in our shape analysis work, which maps the surface onto a planar domain. Surface matching among different individual meshes is achieved by aligning the planar domains of individual meshes. Shape differences of the CC between autistic patients and the controls are computed using Hotelling T^2 two-sample metric followed by a permutation test. The raw and corrected p-values are shown in the results. Additional visualization of the group difference is provided via mean difference map. Copyright © 2009 John Wiley & Sons, Ltd.

Received 7 February 2008; Revised 24 April 2008; Accepted 19 February 2009

KEY WORDS: corpus callosum; autism; shape analysis; planar conformal mapping; permutation test; phenotypic traits

1. INTRODUCTION

A number of studies have documented that autism has a neurobiological basis, but the anatomical extent of these neurobiological abnormalities is largely unknown [1]. Several studies have reported deficits in the size of the corpus callosum (CC) and its sub-regions, although the results are

*Correspondence to: Qing He, Department of Computer Science, University of Missouri-Columbia, Columbia, MO 65211, U.S.A.
†E-mail: qhgb2@mizzou.edu

Contract/grant sponsor: Thompson Center for Autism and Neurodevelopmental Disorders

inconsistent with regard to CC sub-regions. For example, Piven *et al*. [2] reported reductions in the size of the body and posterior regions of the CC in autistic patients, Hardan *et al*. [3] found significant differences in anterior regions, and Vidal *et al*. [1] found reductions in genu and splenium as well as the total CC area. A detailed summary of CC abnormalities in autism can be found in [4]. The inconsistency of the results may be due to factors such as the sample size, subject age and gender, and specific diagnosis. Particularly, heterogeneity within the autism diagnosis obscures the genetic basis of the disorder [5]. Recently, Miles *et al*. proposed a new definition of autism subgroups, which divided autism into essential autism and complex autism [5]. Limiting studies of brain morphology to individuals with essential autism decrease the background noise of structural variation and allow the analysis of the more uniform population [5]. He *et al.* [6] first adopted this definition and compared the shape difference between subjects with essential autism and controls, although their sample size was conspicuously small. In this paper, we also focus on essential autism, which will greatly reduce the heterogeneous factors.

Quantitative morphologic assessment of individual brain structures is often based on volumetric measurements and shape analysis. Shape analysis has gained an increasing amount of interest from the neuroimaging community because it can precisely locate morphological changes in the pathological structures, which cannot be reflected in volume measurements. A significance map is often computed in shape analysis, which tells how significant the difference is between two groups of structures at each location. However, shape analysis gives little description with respect to the phenotype, which is directly linked to the genetic basis of the diseases. A phenotype is the appearance of visible characteristics of an organism produced by its genes and their interaction with the environment; a phenotypic trait is a visual category of phenotypic variation [7]. Under this definition, CC volume is a trait, but agenesis of the CC is a phenotype. Most of the previous works only focus on the volume measurement. However, there are many other traits that can be defined based on the characteristics of the CC shape.

Shape morphology of the CC in autism has been studied in [1, 6]. In [1], CC thickness (the distance from a medial line) at each surface point was compared between patients and controls. In [6], an average CC model was used as a template and the distance to the template at each point was compared between two groups. However, the shape analysis in both was still in a 2D manner, because the comparison was performed on a contour-by-contour basis.

This paper gives a comprehensive pipeline of the analysis of the CC with respect to the shape, morphology and phenotypic traits in essential autism (Figure 1). The 3D model of the CC is reconstructed from 2D contours of nine sagittal slices as in [1]. We use a newly developed semiautomatic method [8] to segment the CC from 2D MR images. Compared with the manual tracing method in most previous work, our method is faster and more accurate, which will facilitate the following analysis. In the phenotypic trait analysis, volumes of the CC and five sub-regions are compared in a way similar to [1]. CC thickness at each region border is also compared. Moreover, an oriented bounding rectangle of the 2D CC on sagittal magnetic resonance imaging (MRI) is constructed, and the length, width and ratio (length/width) of the bounding rectangle are the MRI traits to be compared between autism and control groups. Since the oriented bounding rectangle of an object is the minimum rectangle that encloses this object, the measurements of the bounding rectangle can give both size and shape information. In the shape analysis, we directly compare the 3D coordinates at each surface point of the CC model using Hotelling T^2 two sample tests [9]. In order to perform this comparison, point correspondence among different individual models must be established. We develop a new planar conformal mapping based on the methods in [10, 11] to map the surface onto a planar domain and thus find a one-to-one point correspondence among different

DOI: 10.1002/cnm

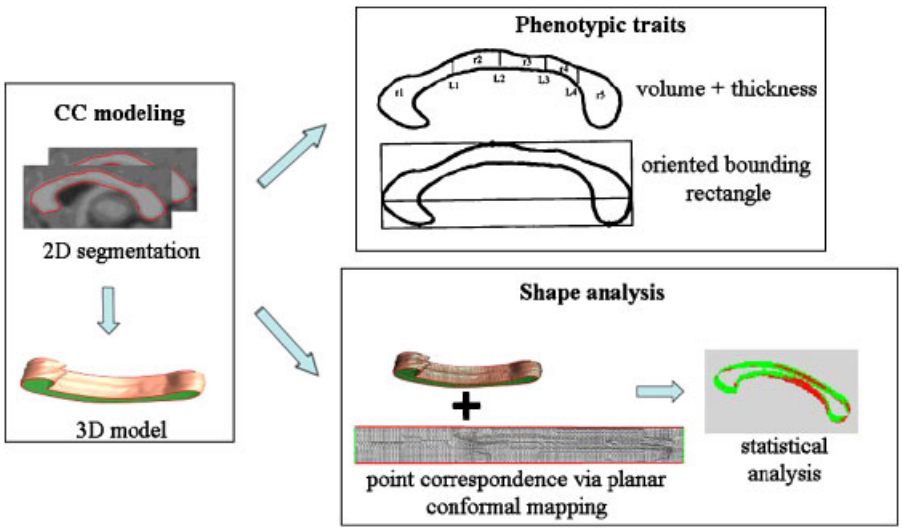

Figure 1. Schematic view of the entire procedure.

models. The results of this paper show both the differences in the phenotypic traits measurements and the visualization of local shape differences between patients and controls.

2. METHODS

This section describes the details of our methods, including CC segmentation, phenotypic trait measurement and statistical shape analysis. The entire procedure can be summarized in the following steps:

1. For each subject, CC contours are segmented from mid-sagittal slice and four adjacent slices on each side, and a 3D model of the CC is constructed by contour stitching.
2. CC volumes and measurements of the oriented bounding box are computed, and differences of these measurements are compared between patients and controls using t-tests.
3. Each CC model is mapped onto a planar domain and re-triangulated to establish the point correspondence among different models.
4. Spatial alignment of all CC models is performed using Procrustes analysis.
5. 3D coordinates at each surface point are compared between patients and controls using Hotelling T2 tests, which results in a significance map of group differences.

The following subsections will describe each step in details.

2.1. CC modeling

We start with slice-by-slice segmentation and stack the 2D curves to make a 3D model. Because, it is more straightforward to verify the accuracy of 2D results slice-by-slice, this method provides better results as opposed to direct 3D segmentation and validation. Mid-sagittal slice and four adjacent slices on each side are used for CC segmentation. The local shape variation of the CC is

DOI: 10.1002/cnm

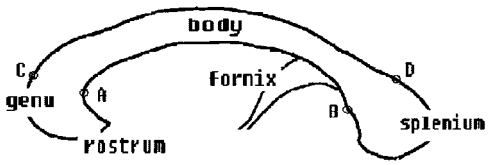

Figure 2. Four parts of the CC boundary: anterior (AC), upper body (CD), posterior (DB), lower body (BA) (image modified based on original illustration from [12]).

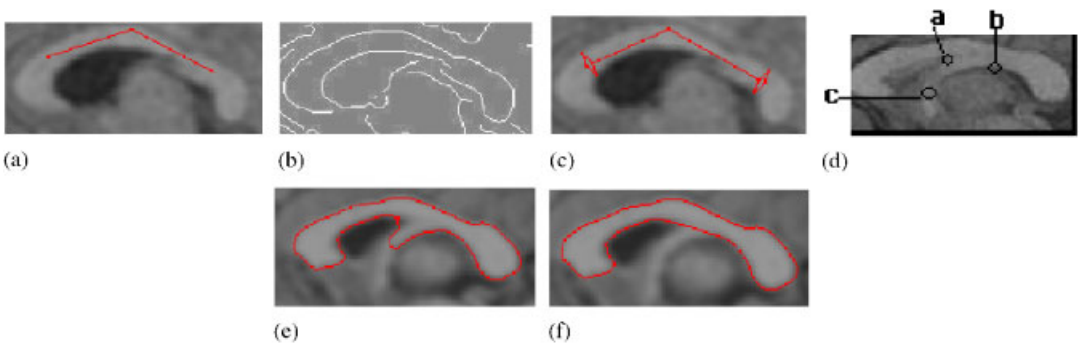

Figure 3. (a) User-initialized polyline; (b) the edge map; (c) the completed seed contour; (d) distinct points around the fornix; (e) the result without fornix removal; and (f) the result with fornix removal.

dramatic, and parts of the CC may be narrow or have bumps. The most challenging problem is the existence of the fornix, which is a thin structure that may or may not contact the CC in sagittal MR images; it is almost the same intensity as the CC. He *et al.* proposed a part-based semiautomatic method [8] to segment the CC on sagittal slices, which can effectively overcome most of the challenges. The novelty of this method is dividing the CC boundary into four parts connected by four sensor points (Figure 2). The user initializes a polyline inside the CC region by three mouse clicks (Figure 3(a)), and a seed contour consisting of four parts is automatically generated by point tracing on the edge map (Figure 3(b) and (c)). The details of the seed construction can be found in [8]. The seed will then automatically deform according to active contour evolution, but each part has its own motion law. The contour evolution mechanism can be found in [8].

The fornix tip can also be removed by automatic fornix detection [8]. Since we know the fornix always appears beneath the body of the CC, we only need to search along the lower boundary to detect it. There are three distinct points around the fornix (Figure 3(d)). The fornix dip is removed by connecting points a and b. The final result on one sagittal slice is shown in Figure 3(f), compared with the intermediate result with the fornix dip in Figure 3(e). The quantitative evaluation of the segmentation results is performed in [8], which shows high accuracy of this method.

Since the CC shapes on adjacent slices do not differ too much, we apply the segmentation method on mid-sagittal slice and the result is used as the seed for its two neighbor slices. After slight deformation, the boundary curves on these two slices can be obtained and each one is again used as the seed of its next adjacent slice.

Contour stitching is performed to create the 3D CC model of each subject. Since the segmentation method can keep track of the four sensor points on the CC boundary, the point correspondence

DOI: 10.1002/cnm

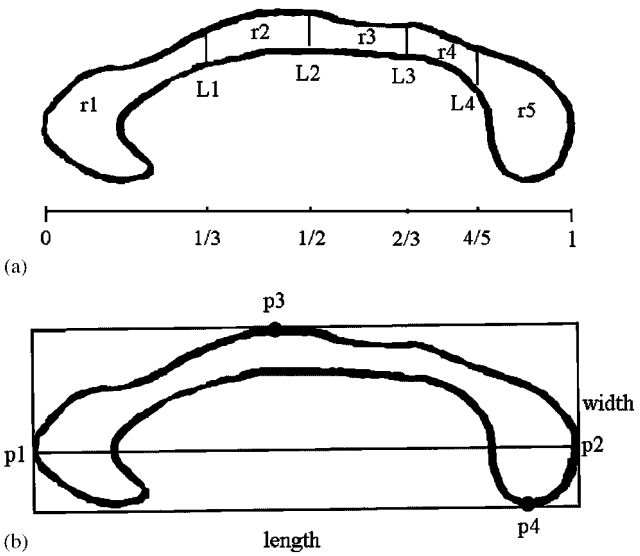

Figure 4. (a) Partition of the CC: r1—anterior third; r2—anterior body; r3—posterior body; r4—isthmus; r5—splenium and (b) bounding rectangle of the CC.

problem can be simplified by first matching the sensor points among contours [6]. After matching the sensor points, the four parts are implicitly matched among contours. We only need to match the individual points within each part. The details of matching the sensor points and the inner points of the four parts can be found in [6].

By connecting the matched point pairs between adjacent contours, the 3D mesh is created. A tangential Laplacian smoothing [13] is performed to maintain a good node distribution of the model. The reconstructed model is shown in Figure 5.

2.2. Phenotypic traits

Volumes of the CC and its sub-regions are computed similar to that in [1]. The CC is divided into five regions along anterior–posterior line (Figure 4(a)). To find the anterior–posterior line, we calculate the distance between every two points on the CC boundary, and find the pair of points with the longest distance (p1 and p2 in Figure 4(a)). The line connecting these two points is the anterior–posterior line. The five regions are defined the same as in [1]. For simplicity, we label them from r1 to r5 as shown in Figure 4(a). Areas are computed in pixels for each 2D segmented CC, and the areas of nine slices are summed to generate the voxel count of the 3D model. The raw volume is the multiplication of the voxel count and the voxel size in mm^3. To take into account the effect of the brain volume, we normalize the raw CC volume by the total brain volume (TBV) and the intracranial volume (ICV), respectively. TBV includes gray matter and white matter and excludes ventricles [14], and ICV is the sum of white matter, gray matter, and inner and outer cerebrospinal fluid spaces [15]. A choice can be made between using TBV or ICV as an adjustment factor [14], but our results show that the two choices do not make any difference. The brain volumes, raw and scaled volumes of the CC and the five regions are compared between patients and controls using *t*-tests.

DOI: 10.1002/cnm

We explore additional phenotypic traits based on the oriented bounding rectangle of the CC. To construct the rectangle, we first find points p1 and p2 as mentioned above. On each side of line p1p2, we find a point on the CC boundary which has the maximum distance to line p1p2 (p3, p4 in Figure 4(b)). The bounding box is a rectangle whose long edges pass p3 and p4, respectively and are parallel to line p1p2, and whose short edges pass p1 and p2, respectively (Figure 4(b)). We measure the length, width and aspect ratio (length/width) of the bounding rectangle on each 2D slice and average them across the nine slices. The shape of the bounding box depends on both the size and the shape of the CC, so these traits can reflect both size and shape information of the CC. We also compute the thickness at the border of every two sub-regions, which is the length of each dividing line (L1–L4 in Figure 4(a)). With a little abuse of notation, we denote the thickness at each dividing border as L1–L4. The thickness at each border is averaged across the nine slices. The average measurements of the bounding box and the thickness are compared between patients and controls using t-tests. To account for the brain volume effect, we scale the above raw measurements by the cubic root of TBV and ICV, respectively. Since these measurements are in millimeter, this scaling makes the units consistent. These scaled measurements are also compared between patients and controls.

2.3. Point correspondence via planar conformal mapping

Conformal parameterization has been explored intensively as a potential approach to the matching and analysis of brain data. It maps the brain surface into regular and more simple domains and carries out the analysis on the parameter domain. Gu *et al*. [11] used spherical conformal map to match cortical surfaces, where they parameterized the genus zero closed surfaces by spheres. Unlike their data, the CC surfaces we are studying have two boundaries, which are the 2D CC contours of the two end slices. Inspired by [10], we design a planar conformal mapping method. In order to find point correspondence among different CC surfaces, we first parameterize each CC surface using a planar domain, and then align the parameterization in the planar domain so that surface points across different objects posses the same parameterization. Finally, the aligned parameterization in the planar domain is mapped back onto the original surfaces (Figure 5).

Among all the CC models an arbitrary model is chosen as the target surface, and the corresponding points on the other models (source surfaces) are to be established to match the points on the target surface. We conformally flatten the target surface M onto a planar domain M', which is a rectangle with the two boundaries γ_1 and γ_2 mapped to the upper and lower long edges. In order to parameterize the given surface with a planar domain, we need to construct a special

Figure 5. Illustration of establishing point correspondence via planar conformal mapping: two individual CC models (left) and their planar domains (right).

DOI: 10.1002/cnm

holomorphic one-form $\tau+\eta\sqrt{-1}$, such that its integration around the boundaries has a real part with a constant period, while the integration along a path from one boundary to the other has a constant imaginary part. To get the imaginary part η, we need to compute a harmonic function f by solving a Dirichlet problem:

$$\begin{aligned} \Delta f &= 0 \\ f|_{\gamma_1} &= 1 \\ f|_{\gamma_2} &= 0 \end{aligned} \tag{1}$$

η is the gradient of f and the real part τ is the conjugate of η. In our implementation, we first convert η into a piece-wise constant vector field υ_η sampled at each face; rotate υ_η by 90° around the face normal, and turn the rotated vector field into the one-form τ. Choosing an appropriate starting point, we can integrate the holomorphic one-form $\tau+\eta\sqrt{-1}$ on M. Taking the real and imaginary parts of the integration to be y and x coordinates, respectively, we get a horizontal strip that is periodic along the X direction. Cutting the strip along the vertical line $x=0$, we get the final planar domain M', where the upper and lower side corresponds to the two boundaries in the original mesh M. The map from M to M' is conformal; the height–width ratio of the rectangle is a conformal invariant of the original surface. In our experiments, we always re-scale the rectangle uniformly along the X and Y directions so that the width equals to 2π. As a consequence, the intrinsic structure is solely reflected by the height of the rectangle for our cases.

The same method is used to map each source surface onto its planar domain. After that, we compute the map between the target planar domain and each source planar domain. In our case, a reasonable map should satisfy two constraints. First, each boundary of the source surface should be aligned with the corresponding boundary of the target surface. In the rectangle domain, we need to map the upper (lower) edge of the source rectangle to the upper (lower) side of the target rectangle. As mentioned before, the width of the rectangle is always equal to 2π, while the height may be different from model to model. Therefore, we may need to re-scale one rectangle along the Y direction to align with the other rectangle. In our experiments, all the rectangles have similar heights, so the re-scaling factor is very close to one and therefore would not hurt the conformality of the map too much. Even in the case of a bigger re-scaling factor, the map is still affine and therefore harmonic, which is already strong enough for our purpose. The second constraint is to align the 'bending corner' (i.e. point c in Figure 2(d)) across two surfaces. In order to make the mapping process easier, we choose the bending corner to be the starting point used in the integration of the holomorphic one-form. As a consequence, in the planar domain the bending corner will appear at the vertical cutting side. Aligning the two rectangles along their left and right sides, the bending corners will be automatically matched. Since all the rectangles have the same width 2π, we do not need to re-scale any of them along the X direction.

Once the source rectangle is totally aligned with the target one, we get a map F' between two planar domains. For each vertex v on the target rectangle, there is a point $F'(v)$ in the source rectangle, which may lie inside a triangle, on an edge or at a vertex. Without loss of generality, we represent the point as a linear combination $F'(v)=b_0v_0+b_1v_1+b_2v_2$, where v_i is the vertex of the resident face and b_i the corresponding barycentric coordinate. The map F' between two planar domains induces a map F between the two original surfaces. Namely, each vertex v in the target surface corresponds to a point $F(v)=b_0v_0+b_1v_1+b_2v_2$ in the source surface. To facilitate later processing, we re-sample the source surface using these points as vertices, and re-triangulate

DOI: 10.1002/cnm

the source surface with the same connectivity as that of the target surface. Therefore, each point on the source surface has a correspondence on the target surface, and the two surfaces have the same triangulation.

The same method is used to align each source planar domain with the target planar domain, and to re-triangulate the source surface. In this way, the point correspondence among all the surfaces is established through the target surface.

2.4. Spatial alignment

Before the shape comparison, rigid-body Procrustes Analysis [16] is performed on each 3D mesh across subjects in order to eliminate the shape differences caused by translation, rotation and scaling. The algorithm can be summarized as follows:

1. Select one shape to be the approximate mean shape (e.g. the shape of the first subject).
2. Align each shape with the approximate mean shape:
   (a) Translate each shape so that its centroid is at the origin.
   (b) Normalize each shape X by a scale factor $s = \|X\|$, where X is the coordinate matrix consisting of row vectors of the coordinate of each point after translation.
   (c) Rotate each shape to align with the newest approximate mean shape. The details of the rotation algorithm can be found in [16].
3. Calculate the new approximate mean shape from the aligned shapes. If it is different from the one in step 2, return to step 2.

2.5. Statistical testing of group mean differences

The difference in the size of the CC has been eliminated in the spatial alignment, so the shape analysis only reveals pure shape difference in local CC area between patients and controls. In the local shape analysis, difference between groups at every surface location is tested (Figure 6). This can be done in two main ways [9]. One way is to analyze the local difference to a template, which

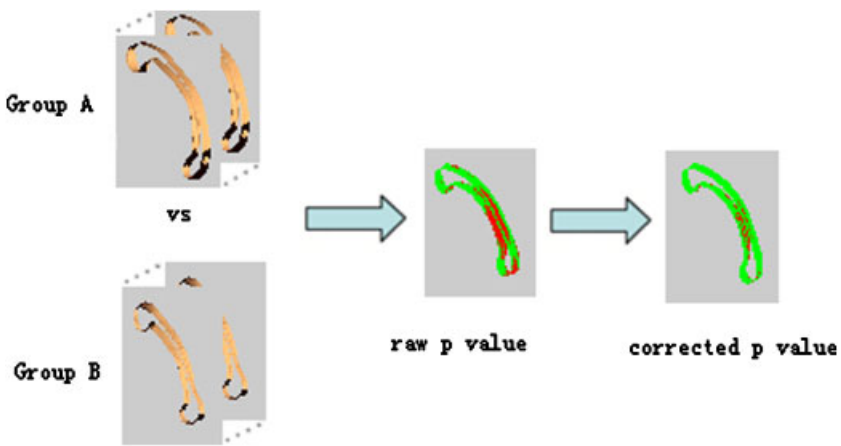

Figure 6. Schematic view of the test procedure.

DOI: 10.1002/cnm

is usually the mean of the two groups. Student t-test can be used to test the local significance and He *et al*. [6] used this method. The main disadvantage of this method is the need to select a template, which introduces an additional bias. The other method is to directly analyze the spatial location of each point, and we apply this method in our study. No template is needed in this approach and multivariate statistics of the (x, y, z) location are used. Hotelling T^2 two-sample metric is used to measure how two groups are locally different from each other. We use a modified T^2 metric instead of the standard one, because it is less sensitive to group differences of the covariance matrixes and the sample size [9]. This metric is defined as

$$T^2 = (\mu_1 - \mu_2)' \left((1/n_1) \sum_1 + (1/n_2) \sum_2 \right)^{-1} (\mu_1 - \mu_2) \tag{2}$$

where $\sum_1$ and $\sum_2$ are the covariance matrices of the two groups. Since comparisons are made at thousands of CC surface points, a permutation test is, therefore, used to confirm the significance of the overall differences in the statistical mapping result adjusting for multiple comparisons [17]. Suppose we have two groups A and B whose sample sizes are n_A and n_B, the permutation scheme can be stated as follows:

1. Calculate the test statistic (in our case, T^2) between A and B, denoted as S_0.
2. The observations of A and B are pooled. From the pooled values, n_A observations are sampled without replacement to form group A, and n_B observations are sampled to form group B. The test statistic between the two new groups is calculated.
3. Repeat the sampling process (permutation) in step 2 for M times. The test statistic in jth permutation is denoted as S_j.
4. The proportion of S_j's, which are greater than S_0 is the p-value.

M is a large number with the maximum value of

$$\binom{n_A + n_B}{n_B}$$

The resulting p-values generate a significance map that locates significant shape differences between the two groups. Both raw and corrected p-values are shown in the experiment.

We also perform a global shape analysis, where the average of the local Hotelling T^2 metrics across the whole surface is calculated for each subject, and the p-value is computed in the same way as for the local testing. No permutation is needed since there is only one test.

3. RESULTS

3.1. Subjects and data

Thirty patients with essential autism participated in this study. All patients met the DSM-IV criteria [18] as well as autism diagnostic interview-revised (ADI-R) and ADOS algorithm criteria. The distinction between essential and complex autism is based on the presence of generalized dysmorphology, which is indicative of an insult to early embryologic development and has been previously reported [5]. Children with a known disorder such as Fragile X, Tuberous Sclerosis, a chromosome abnormality or severe prematurity with brain damage and children with IQs/DQs

DOI: 10.1002/cnm

Table I. Volume measures.

CC measure	Patients	Controls	p-value
TBV (cm^3)	1421.9±299.4	1313.6±336.0	0.09
ICV (cm^3)	1460.4±308.3	1348.3±345.5	0.09
Raw measures	(mm^3)		
Total CC	4229.1±755.3	4727.7.0±971.4	0.01
r1	1754.2±321.3	1939.5±367.9	0.02
r2	474.4±103.9	556.1±142.9	0.008
r3	439.7±123.1	505.1±139.9	0.03
r4	404.6±108.3	458.8±140.8	0.05
r5	1153.3±227.7	1263.5±275.7	0.05
Scaled by TBV	($\times 10^{-4}$)		
Total CC	31.0±9.3	37.0±8.1	0.004
r1	13.0±3.5	15.1±3.1	0.004
r2	3.4±1.0	4.3±1.0	0.001
r3	3.2±1.2	3.9±1.0	0.009
r4	2.9±1.0	3.6±0.9	0.01
r5	8.6±2.9	10.1±2.4	0.02

less than 40 will be excluded. Five healthy people recruited from the NIH Human Brain Project participated as controls. Besides, we also obtained MR images of 23 controls from IBSR database [19]. The age range of all participants is 3–30.

MR images of our patients and controls were obtained from our autism aesthesia protocol, which included intravenous infusion of protocol to insure image quality. Axial, coronal and sagittal T1-weighted images were acquired using the Siemens Symphony 1.5 T scanner with the following parameters: TR = 35 ms, TE = minimum ms, NEX = 1, flip-angle = 30°, thickness = 1.5 mm, field of view = 22 cm, matrix = 512 × 512. The data obtained from IBSR were T1-weighted MR images with 3.1 mm thickness. Each brain volume was interpolated to 0.9 mm isotropic voxels.

3.2. Phenotypic trait measurements

Table I shows the t-test results of the volumes. The mean TBV and ICV of the patients are greater than those of the controls, but the p-values do not reveal any significance in this difference ($p > 0.05$). The raw measures of the CC volume and its sub-regions show that the patient's volume is significantly smaller than the controls ($p <= 0.05$), especially in the region r2 (anterior body). The comparison of the scaled measures by TBV and by ICV shows similar results, both of which augment the significance of the difference. Table I only shows the results of TBV normalization.

Table II gives the t-test results of the traits regarding the bounding rectangle and the thickness. In the raw measures, the patients have significantly reduced length and aspect ratio of the bounding rectangle, while other traits do not show any significance in the difference between patients and controls. When scaled by the cubic root of TBV, the length of the bounding rectangle keeps its strong significance and the width still shows no significance in the group difference. The p-values of the difference in thickness are decreased but none of them reach the significance level (0.05). The difference in L2 between patients and controls is close to significant, which is consistent with the volume measurements since the anterior body displays most significant difference. The comparison shows similar results when the measurements are scaled by the cubic root of ICV, and Table II only shows the results of TBV normalization.

DOI: 10.1002/cnm

Table II. Phenotype traits.

CC measure	Patients	Controls	p-value
Length	66.2±4.8	72.1±5.0	$<10^{-4}$
Width	24.0±3.0	23.6±3.6	0.33
Length/width	2.78±0.3	3.11±0.49	0.002
L1	5.91±1.13	6.09±1.19	0.28
L2	5.40±1.18	5.76±1.35	0.14
L3	5.11±1.35	5.29±1.53	0.31
L4	7.53±1.76	7.77±2.06	0.32
Scaled by TBV			
Length	0.59±0.05	0.66±0.06	$<10^{-4}$
Width	0.21±0.02	0.22±0.03	0.35
L1	0.053±0.011	0.056±0.010	0.14
L2	0.048±0.011	0.053±0.011	0.07
L3	0.045±0.012	0.048±0.013	0.20
L4	0.067±0.016	0.071±0.017	0.22

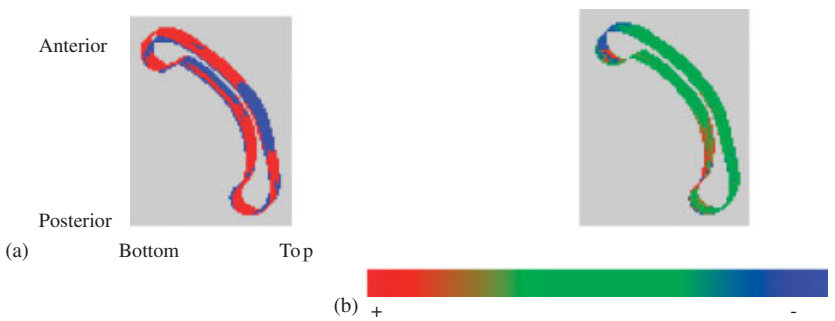

Figure 7. (a) Overlaid average structures (blue: controls, red: patients) and (b) distance map between the two averages.

3.3. Group mean difference map

Figure 7 gives a descriptive visualization of the group difference. The overlaid average CC structures are shown in Figure 7(a). Figure 7(b) shows the signed distance map between the two average structures rendered on an overall average shape, where the negative distances indicate that the patients' structure is outside the controls and the reverse is for the positive distances. The anterior is more projected and the posterior is more inward in the patients' structure. The posterior body and isthmus are thinner in the patients' structure.

3.4. Statistical testing results

The significance maps of the raw and corrected p-values are shown as color coded p-values in Figure 8. Smaller p-values indicate larger statistical significance. A two-tailed alpha level of 0.05 is chosen as the significance threshold. Figure 8(a) is the significance map of raw p-values, which reveals significant difference in the anterior most, anterior body, isthmus and posterior bottom.

DOI: 10.1002/cnm

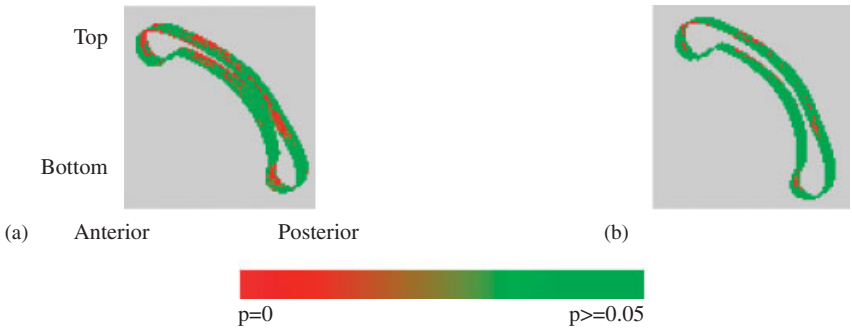

Figure 8. Significance map: (a) raw p-values and (b) corrected p-values.

This result is an optimistic estimation. The permutation result is shown in Figure 8(b), which retains part of the significance in the raw map. The global shape analysis has a p-value of 0.008.

4. CONCLUSION AND DISCUSSION

Based on the new definition of autism subgroups, we investigate the CC abnormalities in essential autism, and exclude the complex autism group in order to find more homogeneous results. We use a semiautomatic method to segment 2D CC boundaries, and 3D surfaces are reconstructed by contour stitching. Regional volumes and additional phenotypic traits based on the oriented bounding rectangle of the CC are compared between patients and controls. A newly developed planar conformal mapping is used to parameterize the 3D surfaces. Shape comparison is conducted at each surface location using Hotelling T^2 test followed by a permutation test.

In the volume comparison, no significance is found in TBV or ICV between patients and controls, but the non-significant trend for an increase in the brain volumes in patients is consistent with the most previous literatures [2, 3, 20]. The significant reduction in the total CC volume in the patients is consistent with [1]. We find significant reduction in each sub-region of the CC in the patients, but in [1] only a significant reduction in the anterior third was found. Besides the traditional volume test, we also conduct some tests based on the oriented bounding rectangle, which has not been done in the previous work. The length, width, and aspect ratio of the bounding rectangle are measured for comparison. We find significant reduction in the CC length and ratio in the patients, but the difference in the width is far from significant. This gives us some insight that the decrease in the CC volume is caused by the decrease in the anterior–posterior length more than the top–bottom length.

In the shape analysis, the distance map reveals more projected anterior most and inward posterior bottom, as well as the thinner body of the CC in the patients. The raw significance map suggests significant differences in the anterior most, anterior body, isthmus and posterior bottom, while the corrected significance map retains part of the significance in each region shown in the raw map. Table III gives a summary of the findings in [1, 6] and our study regarding the shape differences between autism and control groups. First, our results are similar to [1] in the posterior part, but the result in [6] is opposite. This may be accidental because there is no significance in their result. Second, our result on the anterior part is consistent with [6] but contrary with [1]. This may be

DOI: 10.1002/cnm

Table III. Comparison of the CC shape analysis in different studies.

	Body		Anterior		Posterior	
CC regions	Shape	Significant	Shape	Significant	Shape	Significant
[1]	Less arching	No	More inward	Yes	More inward	Yes
[6]	Less arching	Yes	More projected	No	More projected	No
Our study	Posterior thin	Yes	More projected	Yes	More inward	Yes

explained by the population because [6] and our study exclude both the complex autism while [1] does not. Both [1, 6] have found less arching in the body of the CC in autistic patients, but we have found the body thinner in the posterior half. He *et al*. [6] and our study both find significance in the shape changes of the body, although the changes are different.

The results of this study need to be interpreted cautiously because of several limitations. First of all, the age range of our sample is very wide, which may have some effect on the CC measurements. Second, we exclude the complex autism group as it was done in [6]. However, with the improvements in the surface matching and statistical testing methods compared with [6], our results are more convincing than [6].

In conclusion, patients have a trend for a reduction in the volumes of the total CC and each subregion. Further experiment with larger sample size needs to be done to confirm the significance of these size differences. New phenotypic traits based on the oriented bounding box are studied. The decrease in the anterior–posterior length is found to be the main reason for the CC size reduction. A new surface matching technique is used for shape comparison. The permutation results show significant difference in the anterior most, anterior body, isthmus and posterior bottom. Further studies on different subgroups within autistic patients need to be done, such as male vs female and complex vs essential. These findings will better explain the inconsistent results caused by the population.

ACKNOWLEDGEMENTS

Some of the authors of this paper are supported in part by a research scholarship funded by the Thompson Center for Autism and Neurodevelopmental Disorders. We are very grateful for Dr Evan Boote and Chris Jones for helping us in obtaining the MRI data used in this study.

REFERENCES

1. Vidal CN, Nicolson R, DeVito TJ, Hayashi KM, Geaga JA, Drost DJ, Williamson PC, Rajakumar N, Sui Y, Dutton RA, Toga AW, Thompson PM. Mapping corpus callosum deficits in autism: an index of aberrant cortical connectivity. *Biological Psychiatry* 2006; **60**(3):218–225.
2. Piven J, Bailey J, Ranson BJ, Arndt S. An MRI study of the corpus callosum in autism. *American Journal of Psychiatry* 1997; **154**:1051–1056.
3. Hardan AY, Minshew NJ, Keshavan MS. Corpus callosum size in autism. *Neurology* 2000; **55**:1033–1036.
4. Brambilla P, Hardan A, di Nemi SU, Perez J, Soares JC, Barale F. Brain anatomy and development in autism: review of MRI studies. *Brain Research Bulletin* 2003; **61**:557–569.
5. Miles JH, Takahashi TN, Bagby S, Sahota PK, Vaslow DF, Wang CH, Hillman RE, Farmer JE. Essential vs complex autism: definition of fundamental prognostic subtypes. *American Journal of Medical Genetics* 2005; **135A**:171–180.

DOI: 10.1002/cnm

6. He Q, Duan Y, Miles JH, Takahashi TN. Statistical shape analysis of the corpus callosum in subtypes of autism. *IEEE 7th International Symposium on Bioinformatics and Bioengineering*, Boston, MA, U.S.A., 14–17 October 2007.
7. Shyu C, Green JM, Lun DPK, Kazic T, Schaeffer M, Coe E. Image analysis for mapping immeasurable phenotypes in maize. *IEEE Signal Processing Magazine* 2007; 115–118.
8. He Q, Duan Y, Miles JH, Takahashi N. A context-sensitive active contour for image segmentation. *International Journal of Biomedical Imaging* 2007; **2007**:8. Article ID 24826, DOI: 10.1155/2007/24826.
9. Styner M, Oguz L, Xu S, Brechbuehler C, Pantazis D, Levitt JJ, Shenton ME, Gerig G. Framework for the statistical shape analysis of brain structures using SPHARM-PDM. *Insight Journal—2006 MICCAI Open Science Workshop*, 2006.
10. Gu X, Yau S. Global conformal surface parameterization. *Proceedings of the 2003 Eurographics/ACM SIGGRAPH Symposium on Geometry Processing*, 2003; 127–137.
11. Gu X, Wang Y, Chan TF, Thompson PM, Yau S-T. Genus zero surface conformal mapping and its application to brain surface mapping. *IEEE Transactions on Medical Imaging* 2004; **23**(8):949–958.
12. McInerney T, Hamarneh G, Shenton M, Terzopoulos D. Deformable organisms for automatic medical image analysis. *Medical Image Analysis* 2002; **6**:251–266.
13. Wood Z, Desbrun M, Schroder P, Breen D. Semi-regular mesh extraction from volume. *Proceedings of the Conference on Visualization '00*, 2000; 275–282.
14. O'Brien LM, Ziegler DA, Deutsch CK, Kennedy DN, Goldstein JM, Seidman LJ, Hodge S, Makris N, Caviness V, Frazier JA, Herbert MR. Adjustment for whole brain and cranial size in volumetric brain studies: a review of common adjustment factors and statistical methods. *Harvard Review of Psychiatry* 2006; **14**(3):141–151.
15. Wolf H, Kruggel F, Hensel A, Wahlund L-O, Arendt T, Gertz H-J. The relationship between head size and intracranial volume in elderly subjects. *Brain Research* 2003; **973**(1):74–80.
16. Ross A. Procrustes analysis. *Technical Report*, Department of Computer Science and Engineering, University of South Carolina, SC, 2004. Available from: www.cse.sc.edu/∼songwang/CourseProj/proj2004/ross/ross.pdf.
17. Nicolson R, Devito TJ, Vidal CN, Sui Y, Hayashi KM, Drost DJ, Williamson PC, Rajakumar N, Toga AW, Thompson PM. Detection and mapping of hippocampal abnormalities in autism. *Psychiatry Research*: *Neuroimaging* 2006; **148**:11–21.
18. American Psychiatric Association. *Diagnostic and Statistical Manual of Mental Disorders* (4th edn). Text revision, American Psychiatric Association: Washington DC, 2000.
19. http://www.cma.mgh.harvard.edu/ibsr/.
20. Palmer SL, Reddick WE, Glass JO, Gajjar A, Goloubeva O, Mulhern RK. Decline in corpus callosum volume among pediatric patients with medulloblastoma: longitudinal MR imaging study. *American Journal of Neuroradiology* 2002; **23**:1088–1094.

DOI: 10.1002/cnm